

A convolutional neural-network model of human cochlear mechanics and filter tuning for real-time applications

Deepak Baby, Arthur Van Den Broucke, Sarah Verhulst

Dept. of Information Technology, Ghent University, 9000 Ghent, Belgium

* s.verhulst@ugent.be; deepak.baby@idiap.ch

Abstract

Auditory models are commonly used as feature extractors for automatic speech recognition systems or as front-ends for robotics, machine-hearing and hearing-aid applications. While over the years, auditory models have progressed to capture the biophysical and nonlinear properties of human hearing in great detail, these biophysical models are slow to compute and consequently not used in real-time applications. To enable an uptake, we present a hybrid approach where convolutional neural networks are combined with computational neuroscience to yield a real-time end-to-end model for human cochlear mechanics and level-dependent cochlear filter tuning (CoNNear). The CoNNear model was trained on acoustic speech material, but its performance and applicability were evaluated using (unseen) sound stimuli common in cochlear mechanics research. The CoNNear model accurately simulates human frequency selectivity and its dependence on sound intensity, which is essential for our hallmark robust speech intelligibility performance, even at negative speech-to-background noise ratios. Because its architecture is based on real-time, parallel and differentiable computations, the CoNNear model has the power to leverage real-time auditory applications towards human performance and can inspire the next generation of speech recognition, robotics and hearing-aid systems.

1 Introduction

The human cochlea is an active, nonlinear system that transforms sound impinging on the eardrum via the middle-ear bones to cochlear travelling waves of basilar-membrane (BM) displacement and velocity [1]. Cochlear mechanics and travelling waves are responsible for the hallmark feature of mammalian hearing, namely the level-dependent frequency selectivity [2–5] which results from a cascade of cochlear mechanical filters with center frequencies (CFs) between 20 kHz and 40 Hz from the human cochlear base to apex [6].

Modelling cochlear mechanics and travelling waves has been an active field of research because computational methods can help characterize the mechanisms underlying normal or impaired hearing and thereby improve hearing diagnostics [7, 8] and treatment [9, 10], or inspire machine-hearing applications [11, 12]. One popular model approach is to represent the cochlea as a transmission line (TL) which discretizes the space along the BM and describes each section as a system of ordinary differential equations which approximate the biophysical cochlear filter characteristics (Fig.1a; state-of-the-art model) [13–19]. Analytical TL models represent the cochlea as a cascaded system, i.e., the response of one section depends on the responses of

all previous sections, which makes them computationally expensive, as the filter operations in the different sections cannot be computed in parallel. This computational complexity is even greater when nonlinearities or feedback pathways are included to faithfully approximate cochlear mechanics [15, 20].

This computational complexity is the main reason that real-time applications for hearing-aid [21], robotics [22] and automatic speech recognition applications do not adopt cochlear travelling wave models in their pre-processing. Instead, they use computationally-fast approximations of auditory filtering and need to compromise on key auditory features in that process. A common simplification implements the cochlear filters as a parallel, rather than cascaded, filterbank [23, 24]. However, this architecture fails to capture the natural longitudinal coupling properties of the BM [25] and the generation of otoacoustic emissions [26]. Another popular model, the gammatone filterbank model [27], does not include the stimulus-level dependence of cochlear filtering associated with the role of cochlear outer-hair-cells. And lastly, a number of models simulate the level-dependence of cochlear filtering, but fail to match the performance of TL models [28]: they either simulate the longitudinal cochlear coupling locally within individual filters of the uncoupled filterbank [29] or introduce distortion artifacts when combining an automatic-gain-control type of level-dependence with cascaded digital filters [30–32].

The computational complexity of biophysically realistic cochlear models hence poses a design constraint for the development of human-like machine-hearing applications, and motivated our search for a model that matches performance of state-of-the-art analytical TL models while offering real-time execution. Here, we investigate whether convolutional neural networks (CNNs) can be used for this purpose as this type of neural network can deliver end-to-end waveform prediction [33, 34] with real-time properties [35], and is based on convolutions akin to the filtering process associated with cochlear processing.

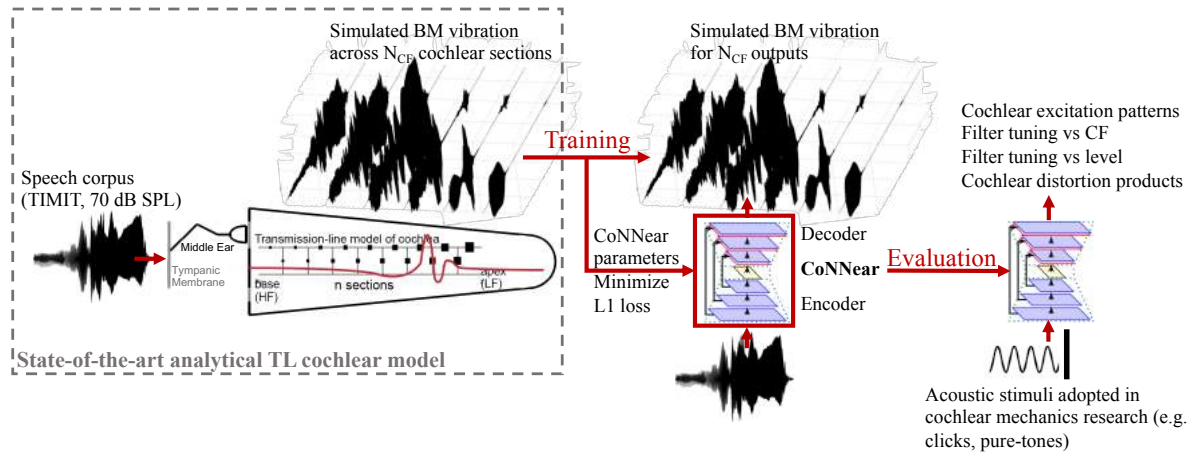
This paper details how CNNs can be best connected and trained to approximate the computations performed by TL cochlear models [19, 36, 37], with a specific emphasis on simultaneously capturing the tuning, nonlinear and longitudinal coupling characteristics of human cochlear processing. The proposed model, namely *CoNNear*, converts speech stimuli into corresponding BM displacements across 200 cochlear filters distributed along the length of the BM. Different from TL models, the CoNNear architecture is based on parallel CPU computations which can be sped up through GPU computing. Consequently, CoNNear can easily be integrated with real-time auditory applications that use deep learning. The quality of the CoNNear predictions and the generalizability of the method towards sound stimuli it did not see during training is evaluated on the basis of cochlear mechanical properties such as filter tuning estimates [38], nonlinear distortion characteristics [39] and excitation patterns [40] using sound stimuli commonly adopted in experimental cochlear mechanics studies.

2 Methods

2.1 CoNNear Architecture

Figure 1(a) illustrates the CoNNear model training and evaluation procedure. While training was performed using TL-model simulated BM vibrations to speech [37], evaluation was performed on the basis of predicting key cochlear mechanical properties using acoustic stimuli it did not see during training. The CoNNear model transforms an acoustic waveform sampled at 20 kHz to N_{CF} cochlear BM displacement waveforms using several CNN layers. CoNNear maps a single acoustic input to N_{CF} outputs, which is different from conventional CNN architectures which map

(a) CoNNear Training and Evaluation



(b) CoNNear Architectures

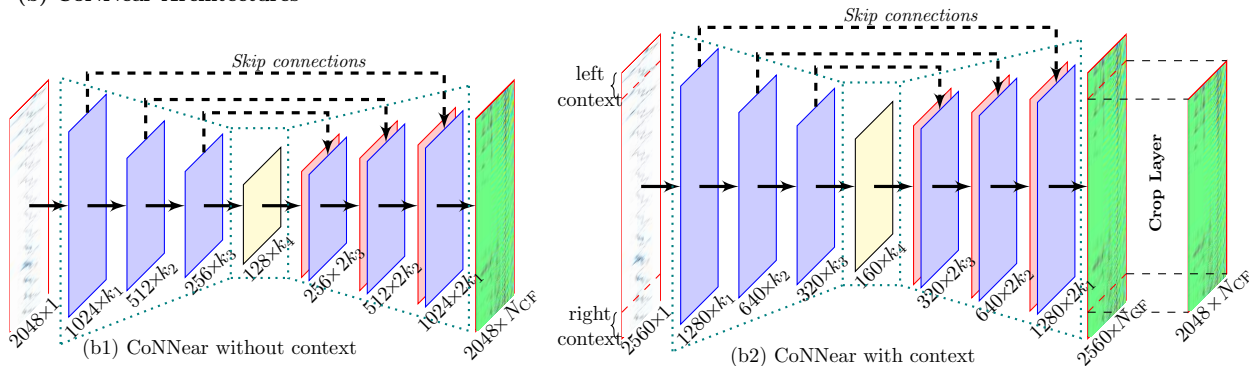


Fig 1. (a) Overview of the CoNNear model training and evaluation procedure. (b) CoNNear architecture with and without context. The final CoNNear model has an autoencoder convolutional neural network architecture which is connected using strided convolutions and skip-connections to map audio input to 201 basilar-membrane vibration outputs in the time-domain. The final CoNNear model has four encoding and decoding layers and a tanh activation function between the layers.

the input to a single output. Every CNN layer is comprised of a set of filterbanks followed by a nonlinear operation [41] and the CNN filter weights were trained on the basis of TL-simulated BM displacements.

Figure 1(b) depicts the CoNNear encoder-decoder architecture: an audio input of length $L = 2048$ is first processed by an *encoder* (comprised of four CNN layers) which encodes the audio signal into a condensed representation of size $128 \times k_4$, after which the *decoder* layers map this representation onto $L \times N_{CF}$. N_{CF} corresponds to 201 BM displacement waveforms (or, cochlear filter outputs) with CFs between 0.1 and 12 kHz. The chosen center frequencies span much of the human hearing range and are spaced according to the Greenwood place-frequency description of the human cochlea [6].

The encoder CNN layers use strided convolutions, i.e. the filters are shifted by a time-step of two such that the temporal dimension is halved after every CNN layer. Thus, after N encoder CNN layers, the audio signal is encoded into a representation of size $L/2^N \times k_N$, where k_N is the number of filters in the N^{th} CNN layer. The decoder uses deconvolution, or transposed-convolutional

layers, to double the temporal dimension after every layer. Additionally, the encoder contains N deconvolution layers to re-obtain the original temporal dimension of the audio input (L). The number of filters in the final decoder CNN layer equals the number of cochlear sections (N_{CF}) simulated in the cochlear TL model, which were used to train the CoNNear parameters.

Temporal alignment, or phase information, of the audio input might be compromised due to the strided convolution operations in the encoder layers. Because preserving temporal information is important for speech perception [42], we used U -shaped skip connections to bypass the temporal audio information to the decoder layers. Skip-connection-based architectures have earlier been adopted for image-to-image translation [43] and speech enhancement applications [33,34] and offer several direct paths between the in- and outputs of CoNNear to maintain the original signal-phase information across the architecture. Skip-connections might also benefit the model when learning how to best combine nonlinearities of several CNN layers to simulate the nonlinear and the level-dependent properties of human cochlear processing.

We trained CoNNear using a fixed length input (here $L = 2048$), but audio applications based on the trained CoNNear will be able to deal with continuous audio inputs as well. This ability to handle variable-duration inputs stems from the convolutional neural-network architecture. In contrast, traditional matrix-multiplication-based neural network architecture can only operate on fixed input duration stimuli. In a general approach, the audio signal could be split into windows of 2048 samples, their corresponding BM displacements simulated, and concatenated. However, because CoNNear treats each input independently, concatenating the simulated outputs would result in discontinuities at the boundaries when there is no context information. To address this issue, we provided context by making the previous L_l and following L_r input samples also available to CoNNear when simulating BM displacement to an input of length L (Fig.1b). Using context, the total input size becomes $L' = L_l + L + L_r$ with an output size of $L' \times N_{\text{CF}}$. A final cropping layer is added to crop out the context ($L_l=L_r=256$ samples) after the last CNN decoder layer. Note that the CoNNear model output units are BM displacement y_{BM} in [μm], whereas the TL-model outputs are in [m]. This scaling was necessary to enforce training of CoNNear with sufficiently high digital numbers. For training purposes, and visual comparison between the TL and CoNNear outputs, the y_{BM} values of the TL model were multiplied by a factor of $10e^6$ in all following figures and analysis.

2.2 Training the CoNNear model

The CoNNear model was trained using TL-model simulations to recordings from the TIMIT speech corpus [44] which contains 2310 phonetically balanced sentences with sufficient acoustic diversity for training. To generate the training data, these 2310 recordings were upsampled to 100 kHz to solve the TL-model accurately [36] and the root-mean square (RMS) energy of every utterance was adjusted to 70 dB sound pressure level (SPL). BM displacements were simulated for 1000 cochlear sections with center frequencies between 25 Hz and 20 kHz using a nonlinear time-domain TL model of the cochlea [37]. From the TL-model output representation (i.e., 1000 y_{BM} waveforms sampled at 20 kHz), outputs from 201 CFs between 100 Hz and 12 kHz, spaced according to the Greenwood map [6], were chosen to train CoNNear. Above 12 kHz, human hearing sensitivity becomes very poor [45], motivating our choice for the upper limit of considered CFs.

Speech material was epoched in windows of 2048 samples for model training and 256 samples were added before and after the input when considering the context model. CoNNear model parameters were optimized to minimize the mean absolute error (dubbed L1 loss) between the

predicted model outputs and the reference TL model outputs. A learning rate of 0.0001 was used with Adam optimizer [46] and the entire framework was developed using the Keras machine learning library [47] with a Tensorflow [48] back-end.

2.3 Evaluating the CoNNear model

Even though CoNNear might end up simulating the speech training dataset with a sufficiently low L1 loss, the quality of the model should be evaluated on its cochlear mechanical properties because CoNNear aims to model cochlear processing. That is, the architecture should also be evaluated on the L1 prediction error to acoustic stimuli of different levels and frequencies used in classical cochlear mechanical studies. This prediction quality was afterwards used to determine the final model architecture and its hyperparameters. The following sections describe the four cochlear mechanics evaluation metrics and their acoustic stimuli. Together, these metrics form a complete description of cochlear processing. Even though any speech fragment can be seen as a combination of basic acoustic elements such as impulses and pure tones of varying levels and frequencies, the basic stimuli associated with the cochlear mechanics evaluation can be considered as *unseen* to the model, as they were not explicitly present in the training material. The evaluation stimuli were sampled at 20 kHz and had a duration of 102.4 ms (2048 samples) and 128 ms (2560 samples) for the CoNNear and context-CoNNear model, respectively. Stimulus levels were adjusted using the reference pressure of $p_0 = 2 \cdot 10^{-5}$ Pa.

2.3.1 Cochlear Excitation Patterns

Cochlear excitation patterns can be constructed from the RMS energy of the BM displacement or velocity at each measured CF in response to tonal stimuli of different levels. Cochlear excitation patterns show a characteristic half-octave basal-ward shift of their maxima as stimulus level increases [40]. Cochlear excitation patterns also reflect the level-dependent nonlinear compressive growth of BM-responses when stimulating the cochlea with a pure-tone of the same frequency as the CF of the cochlear measurement site [3]. Cochlear pure-tone transfer-functions and excitation patterns have in several studies been used to describe the level-dependence and tuning properties of cochlear mechanics [2, 3, 40]. We calculated excitation patterns for all 201 simulated BM displacement waveforms in response to pure tones of 0.5, 1 and 2 kHz frequencies and levels between 10 and 90 dB SPL using:

$$\text{tone}(t) = p_0 \cdot \sqrt{2} \cdot 10^{L/20} \cdot \sin(2\pi f_{\text{tone}} t), \quad (1)$$

where t corresponds to a time vector of 2048 samples, L to the desired RMS level in dB SPL, and f_{tone} to the stimulus frequencies. The pure-tones were multiplied with a Hanning-shaped 10-ms on- and offset ramp to ensure a gradual onset.

2.3.2 Cochlear filter tuning

A common approach to characterize auditory or cochlear filters is by means of the equivalent-rectangular bandwidth (ERB) or Q_{ERB} . The ERB describes the bandwidth of a rectangular filter which passes the same total power than the filter shape estimated from behavioral or cochlear tuning curve experiments [49], and presents a standardized way to characterize the tuning of the asymmetric auditory/cochlear filter shapes. The ERB is commonly used to describe the frequency and level-dependence of human cochlear filtering [4, 50, 51], and Q_{ERB} to describe level-dependent

cochlear filter characteristics from BM impulse response data [19, 52]. To evaluate CoNNear, we calculated Q_{ERB} using:

$$Q_{\text{ERB}} = \frac{\text{CF}}{\text{ERB}}. \quad (2)$$

The ERB was determined from the power spectrum of a simulated BM time-domain response to an acoustic click stimulus using the following steps [52]: (i) compute the Fast Fourier Transform (FFT) of the BM displacement at the considered CF, (ii) compute the area under the power spectrum, and (iii) divide the area by the CF. The frequency- and level-dependence of CoNNear predicted cochlear filters were compared against TL-model predictions and experimental Q_{ERB} values reported for humans [4].

Acoustic stimuli were condensation clicks of 100- μs duration and were scaled to the desired peak-equivalent sound pressure level (dB peSPL), to yield a peak-to-peak click amplitude which matched that of a pure-tone with the same dB SPL level (L):

$$\text{click}(t) = 2\sqrt{2} \cdot p_0 \cdot 10^{L/20} \cdot x(t) \text{ with } x(t) = \begin{cases} 1 & \text{for } t \leq 100 \mu\text{s} \\ 0 & \text{for } t > 100 \mu\text{s} \end{cases} \quad (3)$$

2.3.3 Cochlear Dispersion

Click stimuli can also be used to characterize the cochlear dispersion properties, as their short duration allows for an easy separation of the cochlear response from the evoking stimulus. At the same time, the broad frequency spectrum of the click excites a large portion of the BM. Cochlear dispersion stems from the longitudinal-coupling and tuning properties of BM mechanics [53] and is observed through later click response onsets for BM responses associated with more apical CFs. In humans, the cochlear dispersion delay mounts up to 10-12 ms for stimulus frequencies associated with apical processing [54]. Here, we use clicks of various sound intensities to evaluate whether CoNNear produced cochlear dispersion and BM click responses in line with predictions from the TL-model.

2.3.4 Distortion-product otoacoustic emissions (DPOAEs)

DPOAEs can be recorded in the ear-canal using a sensitive microphone and are evoked by two pure-tones with frequencies f_1 and f_2 and SPLs of L_1 and L_2 , respectively. For pure tones with frequency ratios between 1.1 and 1.3 [55], local nonlinear cochlear interactions generate distortion products, which can be seen in the ear-canal recordings as frequency components which were not originally present in the stimulus. Their strength and shape depends on the properties of the compressive cochlear nonlinearity associated with the electro-mechanical properties of cochlear outer-hair-cells [39], and the most prominent DPOAEs appear at frequencies of $2f_2 - f_1$ and $2f_1 - f_2$. Even though CoNNear was not designed or trained to simulate DPs, they form an excellent evaluation metric, as realistically simulated DPOAE properties would demonstrate that CoNNear was able to capture even the epiphenomena associated with cochlear processing. As a proxy measure for ear-canal recorded DPOAEs, we considered the BM displacement at the highest simulated CF which, in the real ear, would drive the middle-ear and eardrum to yield the ear-canal pressure waveform in an OAE recording. We compared simulated DPs extracted from the FFT of the BM displacement response to simultaneously presented pure tones of f_1 and $f_2 = 1.2f_1$ with levels according to the commonly adopted experimental scissors paradigm: $L_1 = 39 + 0.4L_2$ [56]. We considered f_1 frequencies between 1 and 6 kHz and L_2 levels between 10 and 100 dB SPL.

3 Results

3.1 Determining the CoNNear hyperparameters

An important aspect of this work relates to determining the optimal CNN architecture and associated hyperparameter values. Figure 1(b) shows the final CoNNear layout which resulted from an iterative principled fine-tuning approach in which several hyperparameters were adjusted to achieve the optimal model architecture taking into account: (i) the L1 loss on speech material, (ii) the desired frequency- and level-dependent cochlear filter tuning characteristics, and (iii), the computational load to allow real-time execution. Table 1 details the fixed and variable hyperparameters which were taken into consideration to determine the optimal CoNNear architecture. Tables 2 and 3 compare how different activation functions and layer depths impact the required resources in time and complexity. At the same time, the tables report average L1 losses computed on the training set and on a small set of evaluation metrics. From this crude analysis, we can conclude that an 8-layer CNN architecture yields the best performance across tasks. However, this only forms a rudimentary decision criterion as the final architecture should also capture the subtleties of cochlear mechanics.

To this end, Fig 2 depicts how different activation functions (PReLU: Parametric ReLU [58] or tanh) and layer depths (4,6,8) affected the simulated Q_{ERBS} across the considered CFs. Aside from the reference experimental human Q_{ERB} curve for low stimulus levels [51], simulated Q_{ERB} curves from the reference TL-model (red) with overlaid CoNNear-model simulations are shown. Whereas the PReLU activation function was unable to capture the level-dependence of cochlear filter tuning (i.e. the 40 and 70 dB Q_{ERB} curves overlapped), the tanh nonlinearity was able to simulate both the level and frequency-dependence of human Q_{ERBS} . Fig 2(b) shows that CoNNear captures the frequency-dependence of the Q_{ERB} function better when the layer depth is increased from 4 to 8. Models with 4 and 6 layers underestimated the overall Q_{ERB} and performed worse for CFs below 1 kHz where ERBs were narrower and the corresponding target BM impulse responses were longer than for CFs above 1 kHz. Further increasing the number of layers did not yield a substantial visual improvement over the 8-layer CoNNear model and would further increase the required computational resources. Based on the Q_{ERB} simulations and model performance parameters listed in tables 2 and 3, we chose a final CoNNear architecture with 8 layers and a tanh activation function.

The drawback of adopting a PReLU activation function for cochlear mechanics simulations, is further illustrated when comparing simulated excitation patterns across model architectures. Figure 3 shows that the final model architecture (d) outperforms both architectures without context (c) and the architecture with the PReLU activation function (b). It is important to note that even though both activation functions were able to code negative input deflections, the tanh activation function was the only nonlinearity which captured the nonlinear compression characteristics of cochlear processing. This difference is observed when comparing the peaks of the excitation patterns for different stimulus levels. Whereas the CoNNear-PReLU excitation pattern maxima increased linearly with stimulus level, both the reference TL-model and the tanh-CoNNear excitation patterns showed compressive growth of the pattern maxima. It is hence essential to consider the shape of the activation function (linear growth in PReLU vs compressive growth in tanh) when the reference system is composed of level-dependent nonlinearities. In cochlear mechanics, the properties of the outer-hair-cells are responsible for the nonlinear and compressive growth of BM vibration with stimulus level. Correspondingly, we found that an activation function which resembles the shape of the BM nonlinearity was best able to simulate

Table 1. Overview of the parameters which determine the CoNNear architecture

Fixed parameters	Summary
Window length	The input length was 2048 samples (≈ 100 ms) and $2048 + 2 \cdot 256 = 2560$ samples for the CoNNear-context model.
CNN parameters	The filters in the CNN use a stride of 2 for dimensionality reduction. All CNN layers had a fixed filter length of 64 with 128 filters per layer. The chosen filter length formed an optimal trade-off between the total number of model parameters (and required computations) and performance on the cochlear mechanical tasks.
Number of cochlear output channels	CoNNear was trained to generate BM displacements of 201 cochlear sections with CFs between 100 Hz and 12 kHz according to the Greenwood map [6].
Hyperparameters	Summary
Activation function	The shape of the activation function, or nonlinearity, is crucial to enable CoNNear to learn the cochlear compression properties associated with the role of the outer hair cells (OHCs). To mimic the original shape of the OHC input/output function [57], the activation function should cross the x-axis. Standard activation functions (e.g., sigmoid, ReLUs) do not cross the x-axis, and may end up limiting the CoNNear model from learning realistic level-dependent BM impulse response properties. We hence opted to compare the performance of architectures with activation functions that crossed the x-axis, i.e., the parametric rectified linear unit (PReLU) and hyperbolic-tangent (tanh) nonlinearities.
Number of layers	Increasing the number of layers increases the representational capacity of the model, but evidently also increases the computational complexity (see also Table3). We investigated CoNNear architectures with layer depths of 4, 6 and 8 to determine the minimum model size required to reliably capture the desired cochlear mechanical properties.

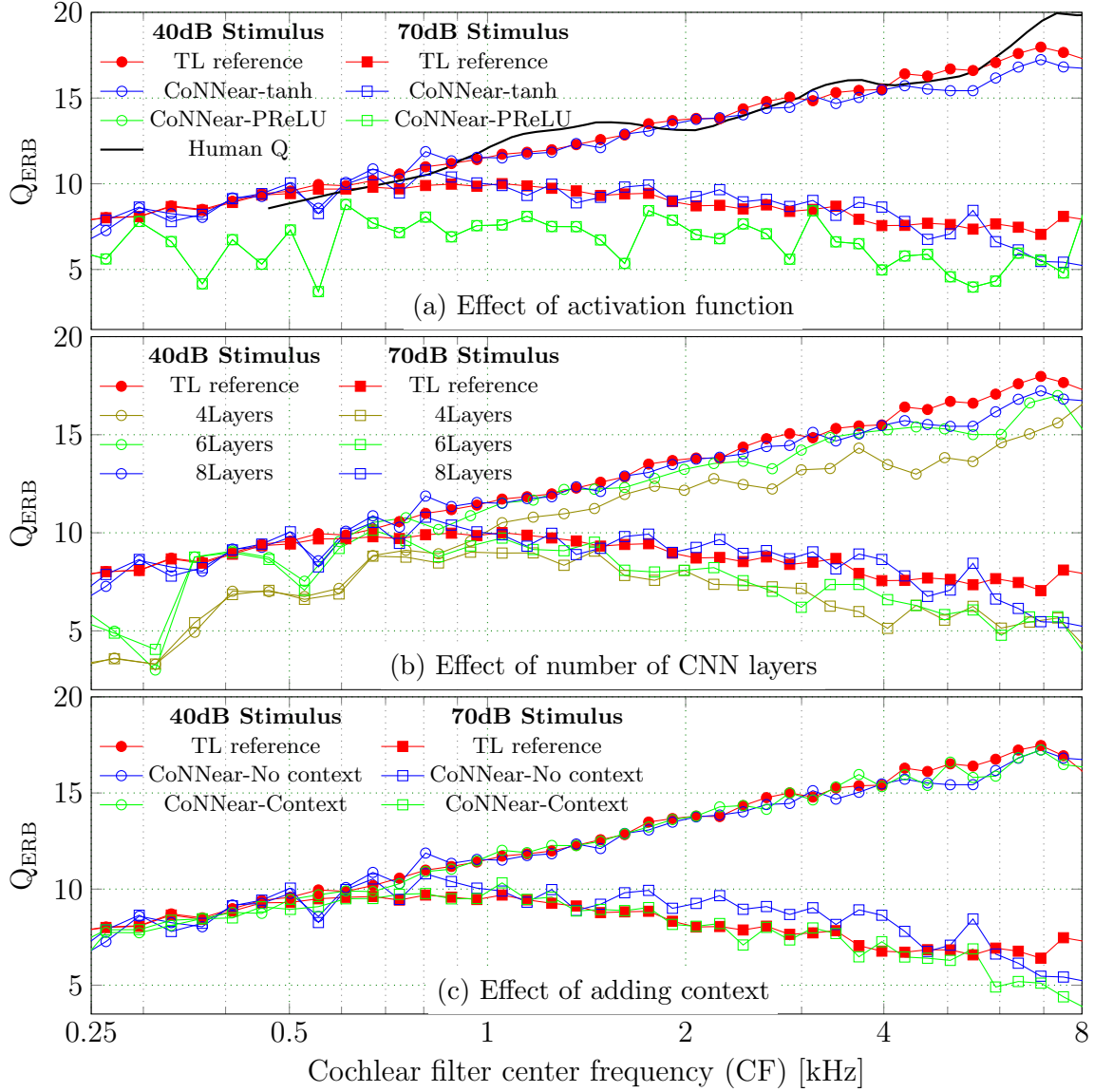


Fig 2. Determining the optimal CoNNear hyperparameters. Simulated Q_{ERB} s across CF were calculated to click stimuli of 40 and 70 dB SPL and are shown for the reference TL model and the CoNNear model in (a), and the CoNNear-context models in (b) and (c). (a) Comparing the PReLU or tanh activation function architectures shows that the PReLU nonlinearity fails to capture level-dependent cochlear filter tuning because the Q_{ERB} functions remained constant despite the stimulus level change. 8 layer CNN architectures were used for this simulation. (b) Increasing the number of CoNNear layers from 4 to 8, improved the Q_{ERB} across CF simulations. (c) Adding context improved the CoNNear predictions by showing less Q_{ERB} fluctuations across CF.

the properties of the analytical TL cochlear model.

Finally, the importance of adding context information is demonstrated in Fig 2c and 4. Figure 2c shows that the reference 70-dB Q_{ERB} s were better captured by the CoNNear model with

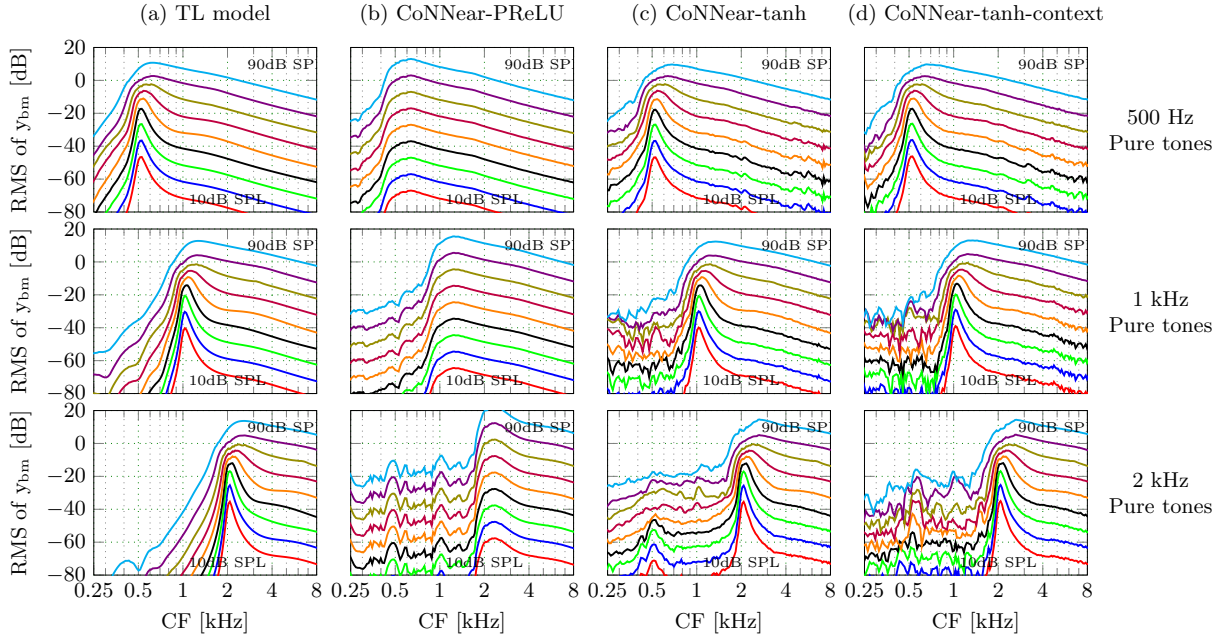


Fig 3. Comparing cochlear excitation patterns across model architectures. Simulated RMS levels of BM displacement across CF for tone stimuli presented between 10 and 90 dB SPL. From top to bottom, the stimulus frequencies were 500 Hz, 1 kHz and 2 kHz, respectively.

context. Figure 4 shows the effect of context on an audiosegment of the TIMIT database which was not seen by CoNNear during training (panel a). Panels b-d show simulated BM displacements of the reference and CoNNear models. It is clear that CoNNear BM displacement predictions show errors at the onset of new stimulus blocks, when context was omitted.

Table 2. Activation function comparison. Number of parameters, time per epoch and obtained L1 loss on the TIMIT training set upon training completion. Average L1 loss values are also computed for CoNNear BM displacement predictions for a number of unseen acoustic stimuli (click and 1 kHz pure tone), for levels ranging between 0 dB SPL and 90 dB SPL and for 32834 stimuli windowed on 192 sentences from the TIMIT test set. The details of the CoNNear architectures are given in the first column. For each evaluated category, the best performing architecture is highlighted in bold font.

Model	#Param	Time/Epoch [h]	Average L1 loss			
			Training set	Click	1kHz	Test set
PReLU/8 lay./no context	11,982,464	1.89	0.0267	0.0126	0.0302	0.0312
tanh/8 lay./no context	11,507,328	1.84	0.0123	0.0023	0.0116	0.0124
tanh/8 lay./context	11,689,984	2.18	0.0087	0.0017	0.0107	0.0081

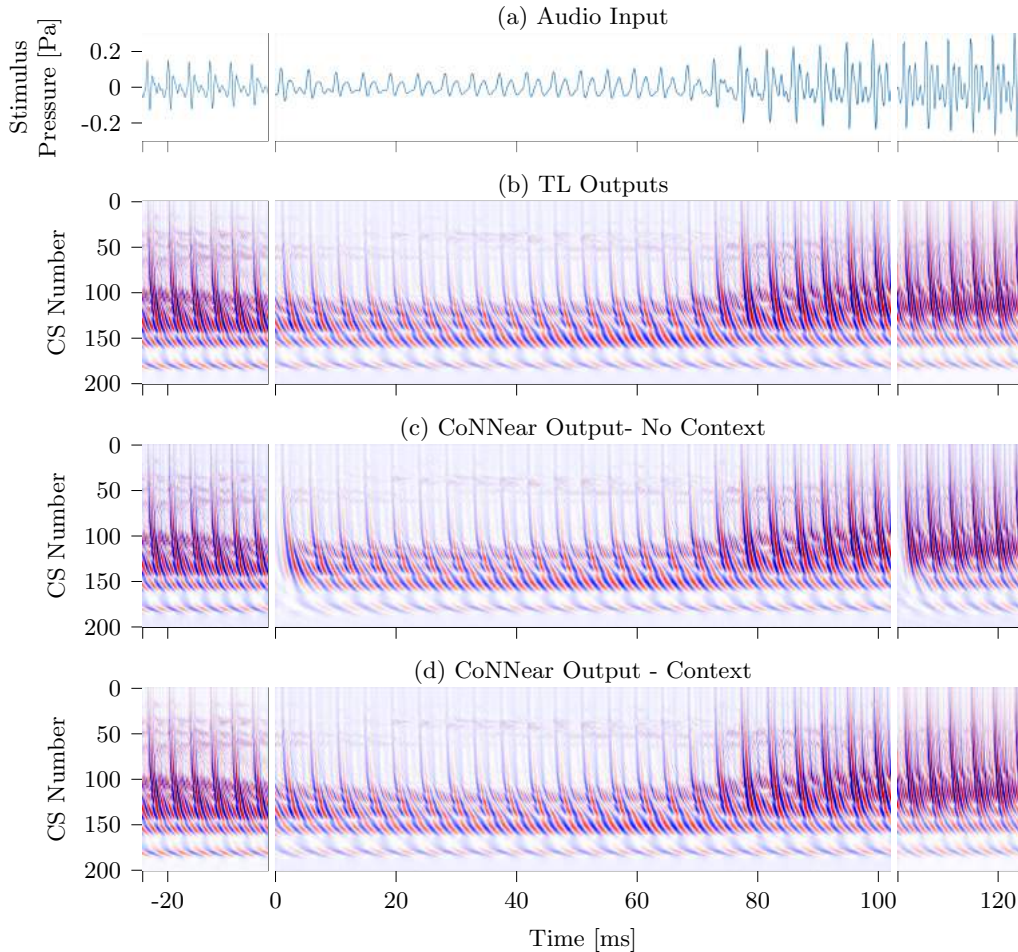


Fig 4. Effect of adding context to the CoNNear simulations. Simulated BM displacements for a 2048-sample-long speech fragment of the TIMIT test set (i.e., unseen during training). The stimulus waveform is shown in panel (a) and panels (b)-(d) depict instantaneous BM displacement intensities (darker colors = higher intensities) of simulated TL-model outputs (b) and two CoNNear architecture outputs: without (c) and with (d) context. The $N_{CF}=201$ output channels are labeled per channel number: channel 1 corresponds to a CF of 100 Hz and channel 201 to a CF of 12 kHz. Intensities varied between $-0.5 \mu\text{m}$ (blue) and $0.5 \mu\text{m}$ (red) for all panels.

3.2 Generalizability of the CoNNear model

Overfitting is a well-known problem in neural network training and occurs when the trained model simply memorizes the training instances and fails to generalize to data that are not present in the training set. We investigated the generalizability of the trained CoNNear model to unseen stimuli from (i) the same database as the training database, (ii) a different database of the same language, (iii) a different database of a different language, and (iv), a music piece.

First, the L1 loss between training and test sentences of the TIMIT database were compared by computing the absolute difference between simulated BM displacements of the TL model and the CoNNear model with context. The histograms of the L1 losses are depicted in Fig 5, and show a similar loss distribution for the training and test data. Notice that the training and test data

Table 3. CNN layer depth comparison. Number of parameters, time per epoch and obtained L1 loss on the TIMIT training set upon training completion. Average L1 loss values are also computed for CoNNear BM displacement predictions for a number of unseen acoustic stimuli (click and 1 kHz pure tone), for levels ranging between 0 dB SPL and 90 dB SPL and for 32834 stimuli windowed on 192 sentences from the TIMIT test set. The details of the CoNNear architectures are given in the first column. For each evaluated category, the best performing architecture is highlighted in bold font.

Model	#Param	Time/Epoch [h]	Average L1 loss			
			Training set	Click	1kHz	Test set
tanh/4 lay./context	5,398,528	2.13	0.0187	0.0035	0.0171	0.0190
tanh/6 lay./context	8,544,256	2.15	0.0102	0.0022	0.0123	0.0105
tanh/8 lay./context	11,689,984	2.18	0.0087	0.0017	0.0107	0.0081

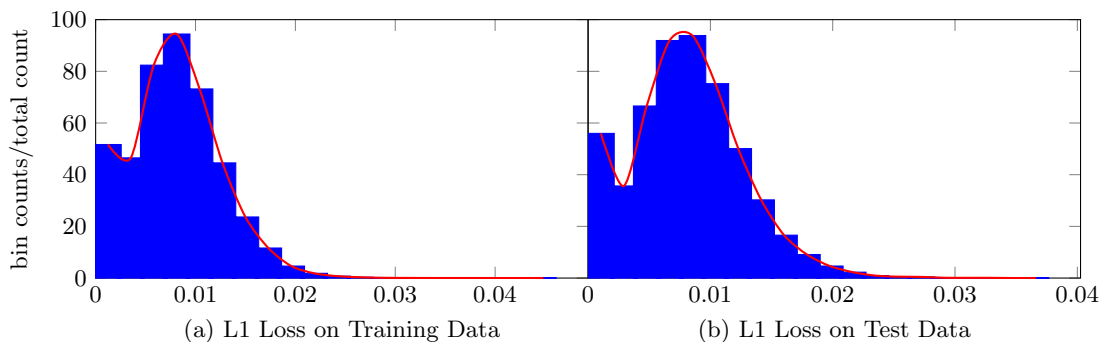


Fig 5. Histograms comparing the L1 losses between TL and CoNNear-context simulations for the TIMIT training (a) and test (b) set. L1 errors were computed for a training set containing 2310 speech sentences, which amounted to 131760 simulated windows of length 2048. The test set contained 550 speech sentences leading to 32834 simulated windows. The pdf functions for both datasets are shown in red.

belonged to different speakers. The trained CoNNear model hence generalizes well to unseen test data of the same TIMIT database.

Next, we investigated how well CoNNear performed on audio stimuli from different databases. Figure 6 compares instantaneous BM displacement intensities between the reference TL-model (b) and CoNNear context model (c) for three stimuli unseen during training: (i) an English sentence from the Wall Street Journal Corpus [59] to investigate the generalizability of CoNNear to different recording settings (first column). (ii) A sentence from the Dutch matrix test [60] to investigate performance on a different language stimulus (middle column), and (iii), a music segment to test performance on a non-speech acoustic stimulus (right column). The simulated intensity differences in panel (d) show that CoNNear generalizes well to a range of unseen testing conditions.

From an application perspective, we tested how well CoNNear could handle audio input of arbitrary length. Fig 7 shows that CoNNear generalizes well to an unseen speech stimulus of length 0.5 s (10048 samples) and a music stimulus of length 0.8 s (16384 samples), even though training was performed using 2048 sample windows.

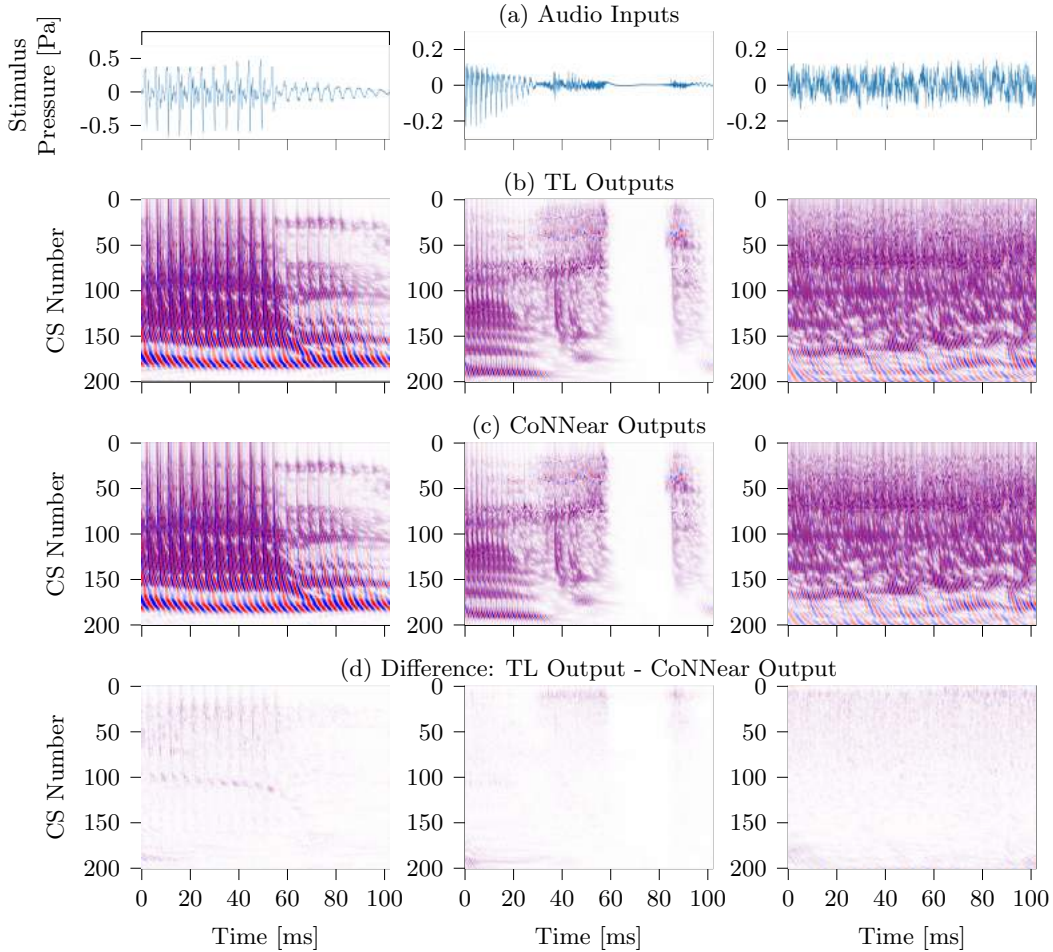


Fig 6. Generalizability of the CoNNear model to unseen audio inputs. Along the columns, simulated BM displacements for three different audio stimuli of 2048 samples length are shown: (i) an English recording from the Wall Street Journal speech corpus [59], (ii) a sentence from the Dutch matrix test [60] and (iii) a music fragment taken from Interpol - Evil. Stimulus waveforms are depicted in panel (a) and panels (b-c) depict instantaneous BM displacement intensities (darker colors = higher intensities) of the simulated TL-model outputs (b) and the CoNNear outputs (c). Panel (d) shows the intensity difference between the TL and CoNNear outputs. The $N_{CF}=201$ considered output channels are labeled per channel number: channel 1 corresponds to a CF of 100 Hz and channel 201 to a CF of 12 kHz. The same color map was used for all figures and ranged between $-0.5 \mu\text{m}$ (blue) and $0.5 \mu\text{m}$ (red).

3.3 Evaluation of CoNNear as a model for human cochlear signal processing

Since the primary goal of this work was to develop a neural-network based model for human cochlear mechanics, this section evaluates how well the trained CoNNear model performs on simulating key cochlear mechanics metrics described in Section 2.3. The level-dependence of simulated cochlear filter tuning was shown in Fig 2, and filter shapes and compression properties were also evident from the pure-tone excitation patterns in Fig 3. The final CoNNear architecture with context (Fig 3 d) captures the reference excitation patterns for different pure-tone frequencies and levels faithfully. However, small excitation pattern fluctuations were observed at CFs below

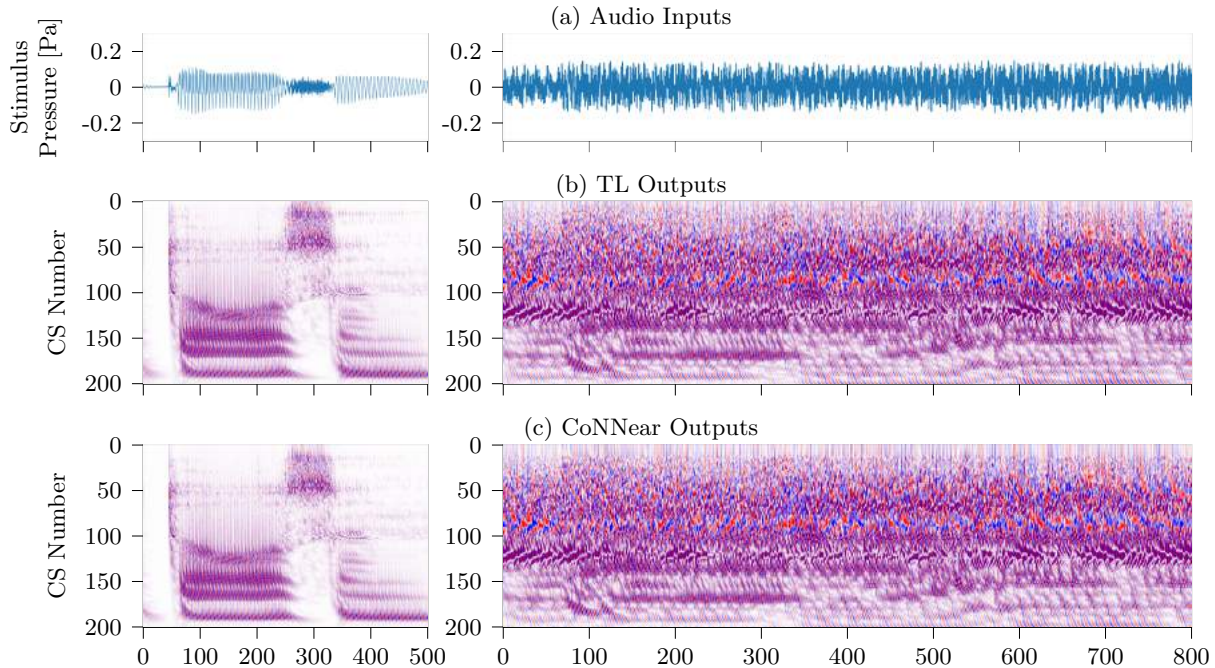


Fig 7. Simulated BM displacements for a 10048-sample-long speech stimulus and a 16384-sample-long music stimulus. The stimulus waveform is depicted in panel (a) and panels (b)-(c) depict instantaneous BM displacement intensities (darker colors = higher intensities) of the simulated TL-model outputs (b) and the CoNNear outputs (c). The $N_{CF}=201$ considered output channels are labeled per channel number: channel 1 corresponds to a CF of 100 Hz and channel 201 to a CF of 12 kHz. The same colorscale was used for both simulations and ranged between $-0.5 \mu\text{m}$ (blue) and $0.5 \mu\text{m}$ (red). The left plot shows simulations to a speech stimulus from the Dutch matrix test [60] and the right plot shows simulations to a music fragment (Interpol - Evil).

the stimulus frequency for the 1 and 2 kHz patterns (middle and bottom row). These spurious fluctuations had levels of approximately 30 dB below the excitation pattern maxima and are hence not expected to impact the sound-driven response of CoNNear to complex stimuli (e.g. such as speech). This latter statement is backed up by the CoNNear speech simulations in Fig 4 which do not show visible noise.

To further quantify the quality of the excitation pattern simulations, we computed the root mean-square error (RMSE) between simulated TL and CoNNear model excitation patterns for a broad range of frequencies and levels in Fig 8. The RMSE was normalized to the TL excitation pattern maximum to obtain a CoNNear error percentage, which remained below 5 % for pure-tone frequencies and levels up to 4 kHz. The error increased for increasing stimulus levels and stimulation frequencies of 8 and 10 kHz. The cause of the larger error percentages can be attributed to the frequency content of the speech material which was used for training. Speech predominantly contains energy below 5 kHz, and we conclude that as long as we use the model for speech-like audio, the error is acceptable. A similar argument can be made for the effect of stimulus level. We used a 70 dB SPL speech corpus to train CoNNear, and hence CoNNear performs best for stimulus levels up to 80 dB SPL. However, it is worthwhile mentioning that the visual difference between simulated high-level excitation patterns was mostly associated with low-level fluctuations

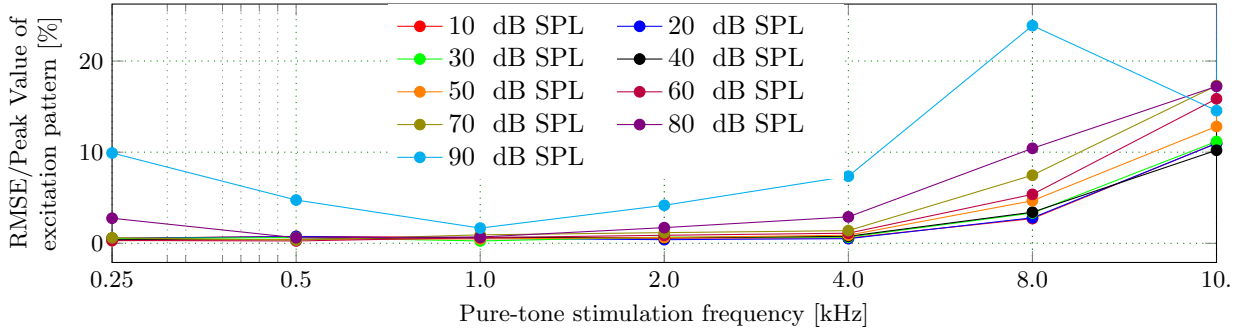


Fig 8. Root mean-square error (RMSE) between simulated excitation patterns of the TL and CoNNear models reported as fraction of the TL excitation pattern maximum (cfr. Fig 3).

at CFs below the stimulation frequency and not at the stimulation frequency itself (i.e. compare first and last column of Fig 3). This means that the stimulus-driven error during simulations with broadband stimuli is likely not affected by these errors as much as is observed here for stimulation with tonal stimuli. To further extend the application range of CoNNear, it is possible to train with higher level stimuli, and/or with extended high-frequency audio content.

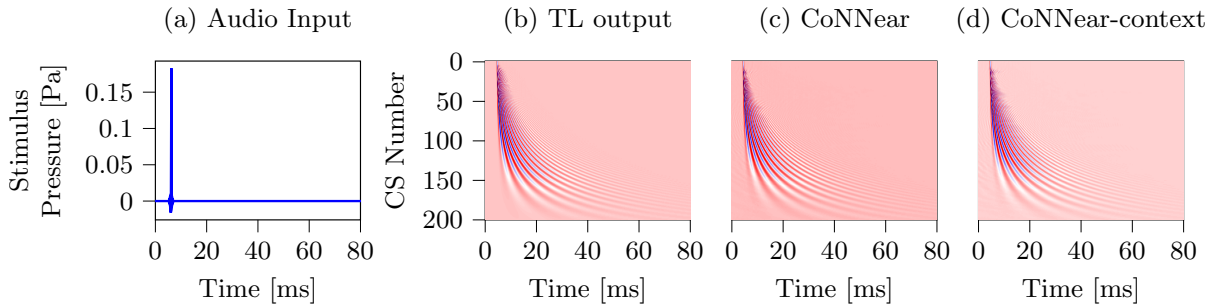


Fig 9. Comparing cochlear dispersion properties. Panel (a) shows the stimulus pressure, while panels (b)-(d) show instantaneous BM displacement intensities for CFs (channel numbers, CS) between 100 Hz (channel 201) and 12 kHz (channel 1). The colorscale is the same in all figure panels, and ranges between $-15 \mu\text{m}$ (blue) and $15 \mu\text{m}$ (red).

Figure 9 depicts the cochlear dispersion characteristics of the TL model and trained CoNNear models and shows the characteristic 12-ms BM displacement onset delay from basal (high CF, low channel numbers) to apical (low CF, high channel numbers) cochlear sections in both models. Cochlear dispersion is a property which arises through the biophysical properties of the BM (i.e. a coupled membrane which has a varying stiffness and damping gradient), and the CoNNear architecture was able to capture this phenomenon. Adding context did not improve the simulations.

To consider a last, key, cochlear mechanics feature, we tested whether CoNNear was able to simulate cochlear distortion products which travel along the BM to generate a pressure waveform in the ear-canal (distortion product otoacoustic emission, DPOAEs). Figure 10 compares the TL-model simulations with those of different CoNNear models (b)-(d). Two factors play a role in determining the optimal CoNNear architecture (d): the shape of the activation function, and the

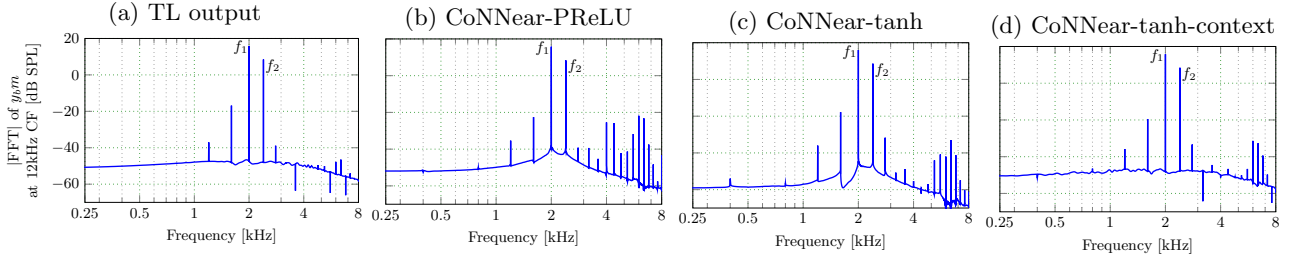


Fig 10. Comparing simulated DPOAEs. The frequency response of the 12-kHz CF channel was considered as a proxy for otoacoustic emissions recorded in the ear-canal. Model simulations are shown in response to two pure tones of f_1 of 2.0 and f_2 of 2.4 kHz. The most pronounced distortion product in humans occurs at $2f_1 - f_2$ (1.6 kHz).

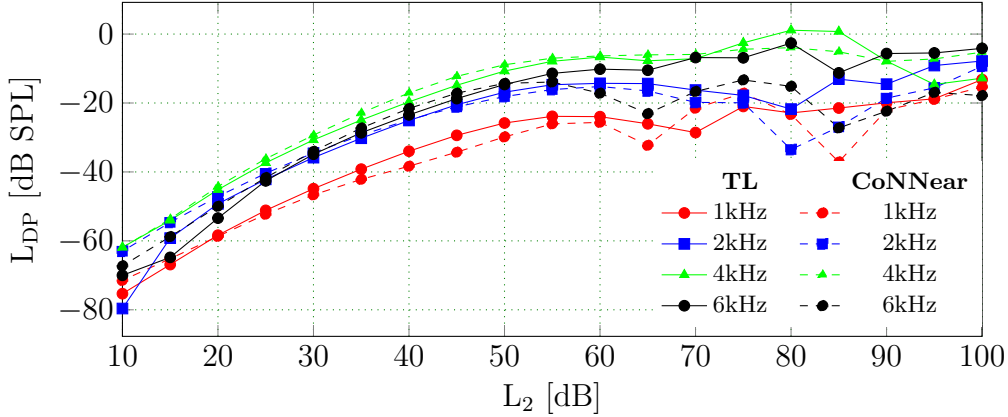


Fig 11. Simulated distortion-product levels (L_{DP}) compared between TL and CoNNear models. L_{DP} was extracted from the frequency response of the 12-kHz CF channel at $2f_1 - f_2$. Simulations were conducted for L_2 levels between 10 and 100 dB SPL, and f_1 between 1 and 6 kHz.

addition of context. DPOAE frequencies are visible from the figure as spectral components which are different from the stimulus primaries of $f_1 = 2.0$ kHz and $f_2 = 2.4$ kHz. The strongest DP component in humans occurs at $2f_1 - f_2 = 1.6$ kHz, and the level of this DP is best captured using the tanh activation function. Secondly, adding context removed the high-frequency distortions that were visible in panels (b) and (c). Again, the activation function which best resembled the shape of the cochlear nonlinearity yielded the best result.

The quality of DPOAE simulations across a range of stimulation levels and frequencies was investigated in Fig 11. Up to L_2 levels of 60 dB SPL, CoNNear matched the characteristic nonlinear growth of both TL-simulated and human DPOAE level functions well [61]. For higher stimulation levels, DPOAE levels started fluctuating in both models. On the one hand, this may reflect the chaotic character of cochlear DPs interacting with cochlear irregularities in TL models and in human hearing [26]. On the other, this may again reflect the limited training material we had available for CoNNear at these high stimulation levels. Given that human DPOAEs are generally recorded for stimulation levels below 60 dB SPL in a clinical or research context [62], we can conclude that CoNNear was able to capture this important epiphenomenon of hearing.

The cochlear mechanics evaluations we performed in Figs. 2, 9, 3, 8, 10 and 11 together demonstrate that the 8-layer, tanh, CoNNear model with context performed best on four crucial aspects of human cochlear mechanics. The stimuli we used for evaluation were not seen during training, to allow for a fair evaluation. Despite training on a limited speech corpus presented at a single RMS level, CoNNear learned to simulate outputs which matched those of biophysically-realistic analytical models of human cochlear processing across level and frequency.

3.4 CoNNear as a real-time model for audio applications

Aside from its realistic cochlear mechanical properties, CoNNear was able to operate in real-time. Real-time is commonly defined as a computation duration less than 10 ms for audio applications (below this limit no noticeable delay is perceived). Table 4 summarizes the necessary time to compute the final CoNNear-context model for a stimulus window of 1048 samples on CPU or GPU architectures. On a CPU, the CoNNear model outperforms the TL-model by a factor of 129 and on a GPU, CoNNear is 2142 times faster. Additionally, the GPU computations show that the final, trained, 8-layer, tanh CoNNear-context model has a latency of 7.27 ms, and hence reaches real-time audio processing performance.

Table 4. Model calculation speed Comparison of the time required to calculate a TL and CoNNear model window of 1048 samples on a CPU (Apple MacBook Air, 1.8 GHz Dual-Core processor) and a GPU (NVIDIA GTX1080). The calculation time for the first window is considered separately for the GPU computations since this window also includes the weight initialization. For each evaluated category, the best performing architecture is highlighted with a bold font.

Model	#Param	CPU (s/window)	GPU 1st window (s)	GPU (ms/window)
PReLU/8 lay./no context	11,982,464	0.222	1.432	7.70
tanh/8 lay./no context	11,507,328	0.195	1.390	7.59
tanh/8 lay./context	11,689,984	0.236	1.257	7.27
Transmission Line	N/A	25.16	N/A	16918

4 Discussion

This paper detailed how a hybrid, deep-neural-net and analytical approach can be used to develop a real-time executable CoNNear model of human cochlear processing, with performance matching that of human cochlear processing faithfully. For the first time, *real-time* and *biophysically-realistic* are not compromised upon, but combined into a single auditory model to inspire a new generation of human-like robotic, speech recognition and machine hearing applications. Prior work has shown clear benefits of using biophysically-realistic auditory models as front-ends for auditory applications: e.g. for capturing cochlear compression, [7, 11, 28], speech enhancement at negative signal-to-noise ratio’s [12], realistic sound perception predictions [63] and for simulating the generator-sources of human auditory brainstem responses [37, 64]. Hence, the CoNNear model can improve performance in application areas which, so far, have refrained from the using slow-to-compute biophysical auditory models. Not only can CoNNear operate on running audio-input with a latency below 7.5 ms, it offers a differentiable solution which can be used in closed-loop systems for auditory feature

enhancement or augmented hearing.

With the rise of neural-network (NN) based methods, computational neuroscience has seen an opportunity to map audio or auditory brain signals directly to sound perception [65–67] and to develop computationally efficient methods to compute large-scale differential-equation-based neuronal networks [68]. These developments are transformative as they can unravel the functional role of hard-to-probe brain areas in perception and yield computationally-fast neuromorphic applications. Key to these breakthroughs is the hybrid approach in which knowledge from neuroscience is combined with that of NN-architectures [69]. While the possibilities of NN approaches are numerous when large amounts of training data are present, this is rarely the case for biological systems and human-extracted data. It hence remains challenging to develop models of biophysical systems which are generalizable to a broad range of unseen conditions or stimuli.

Our work presents a solution to this problem for cochlear processing by constraining the CoNNear architecture and its hyperparameters on the basis of a state-of-the-art TL cochlear model. Our general approach takes the following steps: (i) first, derive an analytical description of the biophysical system on the basis of available experimental data. (ii) Use the analytical model to generate a training dataset to a representative set of sensory stimuli. This training data-set is then used to determine the NN-model architecture and constrain its hyperparameters. Lastly, (iii) as the NN-architecture is trained to match analytical model simulations to a broad range of sensory input features, it is maximally generalizable to unseen inputs. We demonstrated the generalizability of our CoNNear predictions by faithfully predicting key cochlear mechanics features to sounds unseen during training.

Our proposed method is by no means limited to NN-based models of cochlear processing, but can be applied to other nonlinear and/or coupled biophysical models of sensory and biophysical systems. Accurate analytical descriptions of cochlear processing have evolved over the years based on available experimental data from human and animal cochlea, and will continue to improve. It is straightforward to train CoNNear to an updated/improved analytical model in step (i), as well as to include different or additional training data in (ii) to further optimize its prediction performance.

5 Conclusion

We presented a hybrid method which uniquely combines expert knowledge from the fields of computational auditory neuroscience and machine-learning based audio processing to develop a CoNNear model of human cochlear processing. CoNNear presents an architecture with differentiable equations and operates in real time (< 7.5 ms delay) while offering a speed-up factor of 2000 compared to state-of-the-art biophysically realistic models of cochlear processing. We have high hopes that the CoNNear framework will inspire the next generation of human-like machine hearing, augmented hearing and automatic speech recognition systems.

Acknowledgments

This work was supported by the European Research Council (ERC) under the Horizon 2020 Research and Innovation Programme (grant agreement No 678120 RobSpear).

Competing interests

A patent application (PCTEP2020065893) was filed by UGent on the basis of the research presented in this manuscript. Inventors on the application are Sarah Verhulst, Deepak Baby, Fotios Drakopoulos and Arthur Van Den Broucke .

Data availability

The source code of the TL-model used for training is available via [10.5281/zenodo.3717431](https://zenodo.org/record/3717431) or github.com/HearingTechnology/Verhulstetal2018Model, the TIMIT speech corpus used for training can be found online [44]. All figures in this paper can be reproduced using the trained CoNNear model.

Code availability

The code for the trained CoNNear model, including instructions of how to execute it is available from github.com/HearingTechnology/CoNNear_cochlea. A non-commercial, academic UGent license applies.

References

1. von Békésy G. Travelling Waves as Frequency Analysers in the Cochlea. *Nature*. 1970;225(5239):1207–1209.
2. Narayan SS, Temchin AN, Recio A, Ruggero MA. Frequency tuning of basilar membrane and auditory nerve fibers in the same cochleae. *Science*. 1998;282(5395):1882–1884.
3. Robles L, Ruggero MA. Mechanics of the mammalian cochlea. *Physiological reviews*. 2001;81(3):1305–1352.
4. Shera CA, Guinan JJ, Oxenham AJ. Revised estimates of human cochlear tuning from otoacoustic and behavioral measurements. *Proceedings of the National Academy of Sciences*. 2002;99(5):3318–3323.
5. Oxenham AJ, Shera CA. Estimates of human cochlear tuning at low levels using forward and simultaneous masking. *Journal of the Association for Research in Otolaryngology*. 2003;4(4):541–554.
6. Greenwood DD. A cochlear frequency-position function for several species—29 years later. *The Journal of the Acoustical Society of America*. 1990;87(6):2592–2605.
7. Jepsen ML, Dau T. Characterizing auditory processing and perception in individual listeners with sensorineural hearing loss. *The Journal of the Acoustical Society of America*. 2011;129(1):262–281.
8. Bondy J, Becker S, Bruce I, Trainor L, Haykin S. A novel signal-processing strategy for hearing-aid design: neurocompensation. *Signal Processing*. 2004;84(7):1239–1253.

9. Ewert SD, Kortlang S, Hohmann V. A Model-based hearing aid: Psychoacoustics, models and algorithms. *Proceedings of Meetings on Acoustics*. 2013;19(1):050187.
10. Mondol S, Lee S. A Machine Learning Approach to Fitting Prescription for Hearing Aids. *Electronics*. 2019;8(7):736.
11. Lyon RF. *Human and Machine Hearing: Extracting Meaning from Sound*. Cambridge University Press; 2017.
12. Baby D, Van hamme H. Investigating modulation spectrogram features for deep neural network-based automatic speech recognition. In: *Proc. INTERSPEECH*. Dresden, Germany; 2015. p. 2479–2483.
13. de Boer E. Auditory physics. *Physical principles in hearing theory*. I. *Physics reports*. 1980;62(2):87–174.
14. Diependaal RJ, Duijfhuis H, Hoogstraten HW, Viergever MA. Numerical methods for solving one-dimensional cochlear models in the time domain. *The Journal of the Acoustical Society of America*. 1987;82(5):1655–1666.
15. Zweig G. Finding the impedance of the organ of corti. *The Journal of the Acoustical Society of America*. 1991;89:1229–1254.
16. Talmadge CL, Tubis A, Wit HP, Long GR. Are spontaneous otoacoustic emissions generated by self-sustained cochlear oscillators? *The Journal of the Acoustical Society of America*. 1991;89(5):2391–2399.
17. Moleti A, Sisto R, Paglialonga A, Sibella F, Anteunis L, Parazzini M, et al. Transient evoked otoacoustic emission latency and estimates of cochlear tuning in preterm neonates. *The Journal of the Acoustical Society of America*. 2008;124(5):2984–2994.
18. Epp B, Verhey JL, Mauermann M. Modeling cochlear dynamics: Interrelation between cochlea mechanics and psychoacoustics. *The Journal of the Acoustical Society of America*. 2010;128:1870–1883.
19. Verhulst S, Dau T, Shera CA. Nonlinear time-domain cochlear model for transient stimulation and human otoacoustic emission. *The Journal of the Acoustical Society of America*. 2012;132:3842–3848.
20. Zweig G. Nonlinear cochlear mechanics. *The Journal of the Acoustical Society of America*. 2016;139(5):2561–2578.
21. Hohmann V. In: Havelock D, Kuwano S, Vorländer M, editors. *Signal Processing in Hearing Aids*. New York, NY: Springer New York; 2008. p. 205–212.
22. Rascon C, Meza I. Localization of sound sources in robotics: A review. *Robotics and Autonomous Systems*. 2017;96:184–210.
23. Mogran N, Boulard H, Hermansky H. In: *Automatic Speech Recognition: An Auditory Perspective*. New York, NY: Springer New York; 2004. p. 309–338.

24. Patterson RD, Allerhand MH, Giguère C. Time-domain modeling of peripheral auditory processing: A modular architecture and a software platform. *The Journal of the Acoustical Society of America*. 1995;98(4):1890–1894.
25. Shera CA. Frequency glides in click responses of the basilar membrane and auditory nerve: Their scaling behavior and origin in traveling-wave dispersion. *The Journal of the Acoustical Society of America*. 2001;109(5):2023–2034.
26. Shera CA, Guinan JJ. Mechanisms of mammalian otoacoustic emission. In: *Active Processes and Otoacoustic Emissions in Hearing*. Springer; 2008. p. 305–342.
27. Hohmann V. Frequency analysis and synthesis using a Gammatone filterbank. *Acta Acustica united with Acustica*. 2002;88(3):433–442.
28. Saremi A, Beutelmann R, Dietz M, Ashida G, Kretzberg J, Verhulst S. A comparative study of seven human cochlear filter models. *The Journal of the Acoustical Society of America*. 2016;140(3):1618–1634. doi:10.1121/1.4960486.
29. Lopez-Poveda EA, Meddis R. A human nonlinear cochlear filterbank. *The Journal of the Acoustical Society of America*. 2001;110(6):3107–3118.
30. Lyon RF. Cascades of two-pole–two-zero asymmetric resonators are good models of peripheral auditory function. *The Journal of the Acoustical Society of America*. 2011;130(6):3893–3904.
31. Saremi A, Lyon RF. Quadratic distortion in a nonlinear cascade model of the human cochlea. *The Journal of the Acoustical Society of America*. 2018;143(5):EL418–EL424.
32. Altoè A, Charaziak KK, Shera CA. Dynamics of cochlear nonlinearity: Automatic gain control or instantaneous damping? *The Journal of the Acoustical Society of America*. 2017;142(6):3510–3519.
33. Baby D, Verhulst S. SERGAN: Speech Enhancement using Relativistic Generative Adversarial Networks with Gradient Penalty. In: "Acoustics, Speech and Signal Processing (ICASSP), 2016 IEEE International Conference on. Brighton, UK; 2019. p. 106–110.
34. Pascual S, Bonafonte A, Serrà J. SEGAN: Speech Enhancement Generative Adversarial Network. In: INTERSPEECH. ISCA; 2017. p. 3642–3646.
35. Drakopoulos F, Baby D, Verhulst S. Real-Time Audio Processing on a Raspberry Pi using Deep Neural Networks. In: 23rd International Congress on Acoustics (ICA). Aachen, Germany; 2019.
36. Altoè A, Pulkki V, Verhulst S. Transmission line cochlear models: Improved accuracy and efficiency. *The Journal of the Acoustical Society of America*. 2014;136(4):EL302–EL308.
37. Verhulst S, Altoè A, Vasilkov V. Computational modeling of the human auditory periphery: Auditory-nerve responses, evoked potentials and hearing loss. *Hearing Research*. 2018;360:55–75.
38. Oxenham AJ, Wojtczak M. In: Plack C, editor. *Frequency selectivity and masking: Perception*. Oxford University Press; 2010.

39. Robles L, Ruggero MA, Rich NC. Two-tone distortion in the basilar membrane of the cochlea. *Nature*. 1991;349(6308):413.
40. Ren T. Longitudinal pattern of basilar membrane vibration in the sensitive cochlea. *Proceedings of the National Academy of Sciences*. 2002;99(26):17101–17106.
41. LeCun Y, Bengio Y, Hinton G. Deep learning. *Nature*. 2015;521(7553):436–444.
42. Lorenzi C, Gilbert G, Carn H, Garnier S, Moore BC. Speech perception problems of the hearing impaired reflect inability to use temporal fine structure. *Proceedings of the National Academy of Sciences*. 2006;103(49):18866–18869.
43. Isola P, Zhu JY, Zhou T, Efros AA. Image-to-Image Translation with Conditional Adversarial Networks. In: *IEEE-CVPR*; 2017. p. 5967–5976.
44. Garofolo JS, Lamel LF, Fisher WM, Fiscus JG, Pallett DS, Dahlgren NL. DARPA TIMIT Acoustic Phonetic Continuous Speech Corpus CDROM; 1993.
45. *Precise and Full-range Determination of Two-dimensional Equal Loudness Contours*. Geneva, CH: International Organization for Standardization; 2003.
46. Kingma DP, Ba J. Adam: A Method for Stochastic Optimization. *CoRR*. 2014;abs/1412.6980.
47. Chollet F, et al.. Keras; 2015. <https://keras.io>.
48. Abadi M, Agarwal A, Barham P, Brevdo E, Chen Z, Citro C, et al.. TensorFlow: Large-Scale Machine Learning on Heterogeneous Systems; 2015. <https://www.tensorflow.org/>.
49. Moore BC, Glasberg BR. Suggested formulae for calculating auditory-filter bandwidths and excitation patterns. *The journal of the acoustical society of America*. 1983;74(3):750–753.
50. Glasberg BR, Moore BC. Derivation of auditory filter shapes from notched-noise data. *Hearing research*. 1990;47(1-2):103–138.
51. Shera CA, Guinan JJ, Oxenham AJ. Otoacoustic estimation of cochlear tuning: validation in the chinchilla. *Journal of the Association for Research in Otolaryngology*. 2010;11(3):343–365.
52. Raufer S, Verhulst S. Otoacoustic emission estimates of human basilar membrane impulse response duration and cochlear filter tuning. *Hearing research*. 2016;342:150–160.
53. Ramamoorthy S, Zha DJ, Nuttall AL. The biophysical origin of traveling-wave dispersion in the cochlea. *Biophysical journal*. 2010;99(6):1687–1695.
54. Dau T, Wegner O, Mellert V, Kollmeier B. Auditory brainstem responses with optimized chirp signals compensating basilar-membrane dispersion. *The Journal of the Acoustical Society of America*. 2000;107(3):1530–1540.
55. Neely ST, Johnson TA, Kopun J, Dierking DM, Gorga MP. Distortion-product otoacoustic emission input/output characteristics in normal-hearing and hearing-impaired human ears. *The Journal of the Acoustical Society of America*. 2009;126(2):728–738.

56. Kummer P, Janssen T, Hulin P, Arnold W. Optimal L1–L2 primary tone level separation remains independent of test frequency in humans. *Hearing Research*. 2000;146(1):47–56.
57. Russell I, Cody A, Richardson G. The responses of inner and outer hair cells in the basal turn of the guinea-pig cochlea and in the mouse cochlea grown in vitro. *Hearing research*. 1986;22(1-3):199–216.
58. He K, Zhang X, Ren S, Sun J. Delving Deep into Rectifiers: Surpassing Human-Level Performance on ImageNet Classification. In: *IEEE International Conference on Computer Vision (ICCV)*. IEEE Computer Society; 2015. p. 1026–1034.
59. Paul DB, Baker JM. The design for the wall street journal-based CSR corpus. In: *The Second International Conference on Spoken Language Processing, ICSLP*. ISCA; 1992.
60. Houben R, Koopman J, Luts H, Wagener KC, Van Wieringen A, Verschuure H, et al. Development of a Dutch matrix sentence test to assess speech intelligibility in noise. *International Journal of Audiology*. 2014;53(10):760–763.
61. Dorn PA, Konrad-Martin D, Neely ST, Keefe DH, Cyr E, Gorga MP. Distortion product otoacoustic emission input/output functions in normal-hearing and hearing-impaired human ears. *The Journal of the Acoustical Society of America*. 2001;110(6):3119–3131.
62. Janssen T, Müller J. Otoacoustic emissions as a diagnostic tool in a clinical context. In: *Active Processes and Otoacoustic Emissions in Hearing*. Springer; 2008. p. 421–460.
63. Verhulst S, Ernst F, Garrett M, Vasilkov V. Suprathreshold psychoacoustics and envelope-following response relations: Normal-hearing, synaptopathy and cochlear gain loss. *Acta Acustica united with Acustica*. 2018;104(5):800–803.
64. Verhulst S, Bharadwaj HM, Mehraei G, Shera CA, Shinn-Cunningham BG. Functional modeling of the human auditory brainstem response to broadband stimulation. *The Journal of the Acoustical Society of America*. 2015;138(3):1637–1659.
65. Kell AJ, Yamins DL, Shook EN, Norman-Haignere SV, McDermott JH. A task-optimized neural network replicates human auditory behavior, predicts brain responses, and reveals a cortical processing hierarchy. *Neuron*. 2018;98(3):630–644.
66. Akbari H, Khalighinejad B, Herrero JL, Mehta AD, Mesgarani N. Towards reconstructing intelligible speech from the human auditory cortex. *Scientific reports*. 2019;9(1):1–12.
67. Kell AJ, McDermott JH. Deep neural network models of sensory systems: windows onto the role of task constraints. *Current opinion in neurobiology*. 2019;55:121–132.
68. Amsalem O, Eyal G, Rogozinski N, Gevaert M, Kumbhar P, Schürmann F, et al. An efficient analytical reduction of detailed nonlinear neuron models. *Nature Communications*. 2020;11(1):1–13.
69. Richards BA, Lillicrap TP, Beaudoin P, Bengio Y, Bogacz R, Christensen A, et al. A deep learning framework for neuroscience. *Nature neuroscience*. 2019;22(11):1761–1770.